Sensors & Actuators: A. Physical 381 (2025) 116057

Contents lists available at ScienceDirect

Sensors and Actuators: A. Physical

journal homepage: www.journals.elsevier.com/sensors-and-actuators-a-physical

Effects of the passive voltage divider in a photomultiplier tube: Analytical model, simulations and experimental validation

Pablo Martín-Luna [a,*], Daniel Esperante [a,b], José Vicente Casaña [a], Antonio Fernández Prieto [c], Nuria Fuster-Martínez [a], Iris García Rivas [c,d], Benito Gimeno [a], Damián Ginestar [e], Daniel González-Iglesias [a], José Luis Hueso [e], Hannah Andrea Leptin [f], Gabriela Llosá [a], Pablo Martinez-Reviriego [a], Jaime Riera [e], Pablo Vázquez Regueiro [c], Fernando Hueso-González [a]

[a] Instituto de Física Corpuscular (IFIC), CSIC–UV, c/ Catedrático José Beltrán 2, 46980 Paterna, Spain
[b] Electronics Engineering Department, Universitat de València, 46100 Burjassot, Spain
[c] Instituto Galego de Física de Altas Enerxías (IGFAE), Universidade de Santiago de Compostela, Santiagode Compostela, Spain
[d] Triple Alpha Innovation SL, Outes, Spain
[e] Instituto de Matemática Multidisciplinar. Universitat Politècnica de València. Camíde Vera, s/n, 46022 València, Spain
[f] Institute of Physics, Technische Universität Ilmenau, Ehrenbergstraße 29, 98693 Ilmenau, Germany

ARTICLE INFO

Keywords:
Photomultiplier tube
Photodetector
Proton therapy
Passive voltage divider network
Monte Carlo simulation
Gain drift

ABSTRACT

The effects of the passive resistive voltage divider network in a photomultiplier tube (PMT) have been investigated by developing an in-house Monte Carlo simulation code and compared with experimental measurements and an analytical model. The simulation code follows an iterative procedure that takes into account the transport and amplification of the electrons within the device depending on the electrostatic fields produced by the electrode voltages. The PMT gain, dynode voltages, rise time and transit time have been studied as a function of the photocathode current and supply voltage. A good agreement between the analytical model, the simulations and numerous experimental measurements using a Hamamatsu R13408-100 PMT has been obtained. The simulation results endorse the use of logistic functions within the analytical model to account for the collection efficiency in the last dynode stages. This works deepens the understanding of passive voltage dividers and develops an advanced behavioral circuit model of photomultiplier tubes. Although validated for a single PMT, the proposed methodology is applicable to any PMT model. This aids in optimizing the design of fully active voltage dividers, to be applied in extremely pulsed applications with high count rates such as prompt gamma-ray imaging during proton therapy.

1. Introduction

Photomultiplier Tubes (PMTs) are photodetectors with an excellent signal to noise ratio, and the ability to detect down to a single photon in an area as large as 20 square inches [1]. Such devices exploit the photoelectric effect in the cathode and the subsequent amplification of photoelectrons in the dynodes thanks to secondary electrons emission, until the amplified charge is collected in the anode. They are one of the most frequently deployed photodetectors in fields such as nuclear physics, environmental radiation control and life sciences [2] as well as medical imaging and treatment monitoring [3,4].

The behavior of PMTs has been thoroughly investigated from theoretical, semi-empirical and statistical perspectives [1,5,6]. However, the use of equivalent circuit models [7–9] to optimize their voltage supply electronics [10] is less widespread in the scientific community. In particular, the voltage supply of the electrodes of the PMT is usually accomplished with a passive voltage divider, also known as bleeder circuit. It is based on a chain of resistors that divides the total supply voltage according to the ratios recommended by the manufacturer for each dynode.

It is well known that the use of a passive divider is a robust voltage supply solution, albeit not linear with the intensity of illumination. For example, severe variations of the amplification of the PMT as a function of time are observed in PMTs operated in conjunction with scintillation crystals [3] for the monitoring of proton therapy treatments with pencil-beam scanning. These instabilities render the application of PMTs sub-optimal, as complex gain drift correction and threshold adjustment algorithms need to be designed and applied, which degrade

* Corresponding author.
E-mail addresses: pablo.martin@uv.es (P. Martín-Luna), fernando.hueso@uv.es (F. Hueso-González).

https://doi.org/10.1016/j.sna.2024.116057
Received 9 August 2024; Received in revised form 25 October 2024; Accepted 10 November 2024
Available online 20 November 2024

Abbreviations

The following abbreviations are used in this manuscript:

ADC	Analog to Digital Converters
CT	Computed Tomography
DC	Direct Current
MC	Monte Carlo
PCB	Printed Circuit Board
PMT	Photomultiplier Tube
SPICE	Simulation Program with Integrated Circuit Emphasis
SEY	Secondary Electron Yield

the accuracy of the γ-ray spectrometer when operated at very high count rates [11,12].

A common mitigation strategy is to use active voltage dividers, which add transistors to stabilize the voltage in each dynode. Their design is usually optimized in an iterative process, with manufacturing, experimental tests at a beam, and modification of the electronics board. This procedure has two drawbacks: (i) the underlying cause of the gain drifts is not fully understood, and thus its mitigation might not be pinpointed to the optimum component, (ii) the empirical optimization is burdensome, takes time and resources, and might not converge to the best solution.

To cover this gap, recent developments have focused on the design of more accurate behavioral circuits that can be used for fast but also reliable electronics optimization. To validate these equivalent circuits, accurate Monte Carlo modelings of the PMT are needed alongside, and have been recently published [13,14].

In this manuscript, our goals are to:

- derive a circuit model of the passive voltage divider coupled to the electrodes of the PMT, which are described as current sources, and solve the corresponding system of non-linear equations;
- validate the proposed analytical model with accurate Monte Carlo simulations of the PMT geometry and electron transport;
- compare both predictions with experimental measurements on a dynode-by-dynode basis of the gain and timing properties, rather than just a simple end-to-end test of the amplification.

The manuscript is structured as follows. In Sections 2 and 3, we describe the behavioral circuit model and the Monte Carlo (MC) simulation framework, respectively. In Section 4, we explain the technical details of the experimental setup platform. In Section 5, we compare the equivalent circuit model solution and the MC simulation results with experimental measurements to validate the developed methodology, and discuss the study limitations. In Section 6, we summarize the main findings and give an outlook on future research.

2. Analytical model

2.1. Electrode currents

We study a steady-state of an N-stage PMT tube model ($N > 0$), consisting of $N + 2$ electrodes (cathode $i = 0$, dynodes $i \in [1, N]$ and anode $i = N + 1$), supplied by a passive voltage divider network with resistors. Unlike in the physical world, we assume that there is no time sequence or ordering of the interactions in the amplification cascade.

Let us define $\phi_{\mathrm{v},i}$ as the number of electrons per unit of second that escape electrode i into the vacuum tube, and $\phi_{\wedge,i}$ the corresponding flow of electrons stemming from the vacuum and impacting with electrode i. We define ϕ_{k} as the flow of electrons (towards the vacuum) per unit of second produced by the incident light on the photocathode. The associated current entering the vacuum is thus negative: $I_{\mathrm{k}} = -\mathrm{e}\phi_{\mathrm{k}}$, where e is the elementary charge constant.

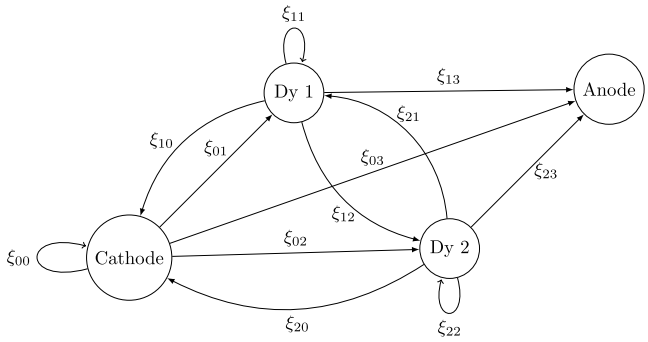

Fig. 1. Scheme of the definition of the elements of the correlation matrix ξ for a PMT with a cathode, 2 dynodes and an anode. The element ξ_{ji} represents the probability that, given a voltage difference between electrodes, one electron emitted from the electrode j reaches the electrode i. The arrows indicate the direction of the movement of the electrons.

In general, the electrons emitted from the electrode j can travel to any other electrode i, including the emitting electrode if $i = j$. This effect can be modeled by a correlation matrix ξ, where the element ξ_{ji} is the probability that an electron emitted from the electrode j into the vacuum arrives at electrode i, cf. Fig. 1, and S_{ji} is the secondary emission coefficient which corresponds to an electron emitted from the electrode j that impacts on the electrode i. Both S and ξ depend on the PMT geometry, material and the effectively supplied inter-electrode voltages. For simplicity, it is assumed that all electrons will eventually arrive to an electrode (i.e. $\sum_{j=0}^{N+1} \xi_{ij} = 1$). Also, second and higher-order contributions are disregarded ($\xi_{ij} S_{ij} \xi_{ji} S_{ji} \ll 1$). Thus, the flow rate of electrons $\phi_{\wedge,i}$ from the vacuum into the electrode i is then:

$$\phi_{\wedge,i} = \sum_{j=0}^{N+1} \xi_{ji} \phi_{\mathrm{v},j}, \quad i \in [0, N+1], \tag{1}$$

and the flow rate of electrons from each electrode into the vacuum $\phi_{\mathrm{v},i}$ after photoelectric or secondary emission is given by:

$$\phi_{\mathrm{v},i} = \begin{cases} \phi_{\mathrm{k}}, & i = 0, \\ \sum_{j=0}^{N+1} S_{ji} \xi_{ji} \phi_{\mathrm{v},j}, & i \in [1, N], \\ 0 & i = N+1 \end{cases} \tag{2}$$

where it is assumed that secondary electrons cannot be emitted from the cathode and the anode ($S_{j0} = S_{j(N+1)} = 0$ for all j).

On the other hand, the current $I_{\mathrm{e},i}$ going through each electrode $i = 0, \ldots, N+1$ towards the voltage divider network is obtained using the Kirchhoff's current law:

$$I_{\mathrm{e},i} = \begin{cases} \mathrm{e}(\phi_{\mathrm{k}} - \phi_{\wedge,0}), & i = 0, \\ \mathrm{e}(\phi_{\mathrm{v},i} - \phi_{\wedge,i}), & i \in [1, N], \\ -\mathrm{e}\phi_{\wedge,N+1}, & i = N+1, \end{cases} \tag{3}$$

where $I_{\mathrm{e},0} \equiv I_{\mathrm{c}} = -I_{\mathrm{k}} - \mathrm{e}\phi_{\wedge,0}$ corresponds to the cathode, $I_{\mathrm{e},N+1} \equiv I_{\mathrm{a}}$ to the anode, and $I_{\mathrm{e},i} \equiv I_{\mathrm{dy},i}$, $i \in [1, N]$ to the dynodes, cf. Fig. 2. Note that $I_{\mathrm{k}} < 0$, $I_{\mathrm{a}} < 0$ and the gain of the PMT is given by:

$$G = \frac{\phi_{\wedge,(N+1)}}{\phi_{\mathrm{k}}} = \frac{I_{\mathrm{a}}}{I_{\mathrm{k}}}. \tag{4}$$

It is worth mentioning that if we assume that the electrons emitted from the electrode i can only travel to the next dynode with an efficiency $\eta_i \equiv \xi_{i(i+1)}$ (the usual case if the effective voltage supply is monotonously increasing with dynode number) or be self-absorbed in the emitting dynode (i.e. $S_{ii} = 0$) with probability $\xi_{ii} \equiv 1 - \eta_i$, then the model is analogous to the one presented in [7], after substituting $S_{i(i+1)} \equiv g_i$ and offsetting by 1 the indices.[1]

[1] A mistake in the equations of the published version [7] was corrected in the institutional repository: https://hdl.handle.net/10550/80331.

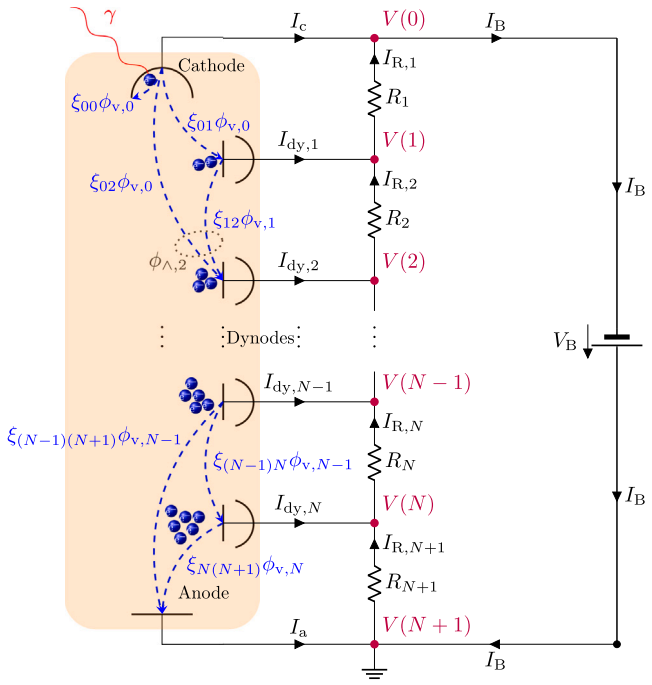

Fig. 2. Schematic of an N-stage PMT connected to a supply voltage V_B in negative polarity mode and a chain of resistors R_i with $i \in [1, N+1]$. The power supply bias current is I_B, and the electrode voltages $V(i)$ are shown for $i \in [0, N+1]$. The vacuum tube consists of $N+2$ electrodes: one photocathode ($i = 0$), N dynodes ($i = 1, \ldots, N$), and one anode ($i = N+1$). The electrode currents are I_c, $I_{dy,i}$, $i \in [1, N]$, and I_a, whereas the current flowing through the resistors is labeled as $I_{R,i}$, $i \in [1, N+1]$. A photon (γ) generates a photoelectron in the cathode. The electrons (small balls) can flow in vacuum to any electrode. The dashed arrows indicate some of the possible directions followed by the electrons and the corresponding flow of electrons per unit of second. $\phi_{v,i}$ is the flux of electrons going away from dynode i, while $\phi_{\wedge,i} = \sum_{j=0}^{N+1} \xi_{ji}\phi_{v,j}$ is the flux of electrons impacting on dynode i, which is illustrated as a dotted ellipse for dynode 2. Note that, for the sake of clarity, we only depict two of the contributions to the sum (the most relevant ones).

2.2. Resistive voltage divider network

A common way to supply the $N+2$ electrodes of an N-stage PMT is to apply the total voltage bias $V_B > 0$ between anode ($i = N+1$, at ground) and cathode ($i = 0$, negative), and to use a chain of $N+1$ resistances R_i ($i = 1, \ldots, N+1$) between electrodes i and $i-1$, as depicted in Fig. 2.

Thus, using the Kirchhoff's current law and the Ohm's law, the system of equations governing the PMT model is given by:

$$\begin{cases} V(0) = -V_B \\ \dfrac{V(i) - V(i-1)}{R_i} = \dfrac{V(i+1) - V(i)}{R_{i+1}} + I_{dy,i} \quad i \in [1, N], \\ V(N+1) = 0\,\text{V} \end{cases} \tag{5}$$

The currents going through each dynode $I_{dy,i}$ are responsible for the non-linearity of the system of equations. It is worth noting that the power supply is connected to ground on the anode, i.e. the PMT is operated with negative polarity. The formalism is also valid when the PMT is operated with positive polarity (cathode is at ground, anode is at positive polarity), as the equations only depend on the voltage differences and not on their absolute value. One just needs to replace the boundaries of Eq. (5) with: $V(0) = 0\,\text{V}$ and $V(N+1) = V_B$.

3. Simulation program

The simulation of the amplification and transport of electrons taking into account the resistive divider network in a realistic PMT geometry is carried out by means of an in-house developed code based on the tracking of an electron within the device, whose motion is governed by the electrostatic field. A comprehensive description of the simulation code is given in [14].

Here, we first briefly summarize the general considerations to perform the simulation for a certain electrode voltages, cf. Section 3.1. We adopt the 2.5D strategy since it is a good approximation in the absence of magnetic fields with a much lower computational cost compared to a 3D simulation [14]. In this strategy, the electrons can move in 3D, but the geometry is assumed to be invariant in the perpendicular direction, so the field calculation can be done in a 2D plane in only one minute with a standard desktop computer and a mesh resolution of 0.05 mm. Second, we describe in Section 3.2 the iterative method developed for including the effect of the resistive divider network.

3.1. General considerations

The 3D computer-aided design modeler FreeCAD [15] has been used to retrace the 3D geometry of the 8-dynode linear-focused ⌀1.5" R13408-100 PMT from Hamamatsu (Hamamatsu, Japan) basing on Computed Tomography (CT) scans as well as direct measurements with a calliper. The 3D geometry is then projected on a 2D plane, which is the one considered when calculating the electrostatic fields. We will consider the resistors displayed in Table 1, whose values follow closely the recommended electrode voltage ratios by the manufacturer [14, Table 1], to provide the voltages to each dynode. The grid and acceleration electrodes are supposed to be passive elements in the presented PMT model, with no current circulating through them.

The simulation code includes the emission of electrons in a PMT, electron transport, emission of secondary electrons and collection in the anode grid. An overview of the simulation code is represented in a flowchart in Fig. 3.

3.1.1. Emission

We assume that photoelectrons are uniformly emitted without kinetic energy from the arc line that models the photocathode. These electrons are emitted from the cathode thanks to the photoelectric effect due to the absorption of optical photons.

3.1.2. Transport

The electron movement in a PMT is mainly affected by the electrostatic field, which depends on the electrode voltages and geometry. The electrostatic fields are calculated using the Poisson Superfish software [17] in a predefined mesh. Then, the electron trajectories are obtained by numerically solving the Lorentz's force motion equation for each electron by means of a *leapfrog* algorithm: the Boris method [18,19] with time steps of 8 ps, neglecting space-charge effects and by interpolating the value of the electrostatic field at the particle's position between mesh points. This procedure allows us to update the electron position and velocity within the PMT.

3.1.3. Secondary emission

After each position update it is checked if the particle impacts on any electrode. When such an event occurs, the interaction between the electron and the metal surface is modeled by calculating the total Secondary Electron Yield (SEY) coefficient S of the material (i.e. the average number of electrons emitted per incident one) using the Modified Vaughan's model [14,20,21]. In this model, the SEY coefficient $S(E, \theta)$ is a function of the impacting electron kinetic energy E and the incident angle θ with respect to the surface normal. In the simulations, we consider that the dynodes 3, 4 and 5 are made of CuBeO and the rest of dynodes of Cs_3Sb. The parameters of the Modified Vaughan's model for these materials can be found in [14, Fig. 3]. It is worth mentioning that we use the parameter $k_\delta = 1.20$ that has been readjusted compared to [14, Section 3.2] because the resistors considered in Table 1 provide voltage ratios which slightly differ from the recommended values.

Table 1
Resistors between cathode, grid, dynodes, acceleration electrode (Acc), and anode of the ⌀1.5" R13408-100 PMT.

Electrodes	Cathode	Grid	Dy1	Dy2	Dy3	Dy4	Dy5	Dy6	Dy7	Dy8 (Acc)	Anode
R (MΩ)	12.7	46.9	15	15	10	10	10	10	10	10	

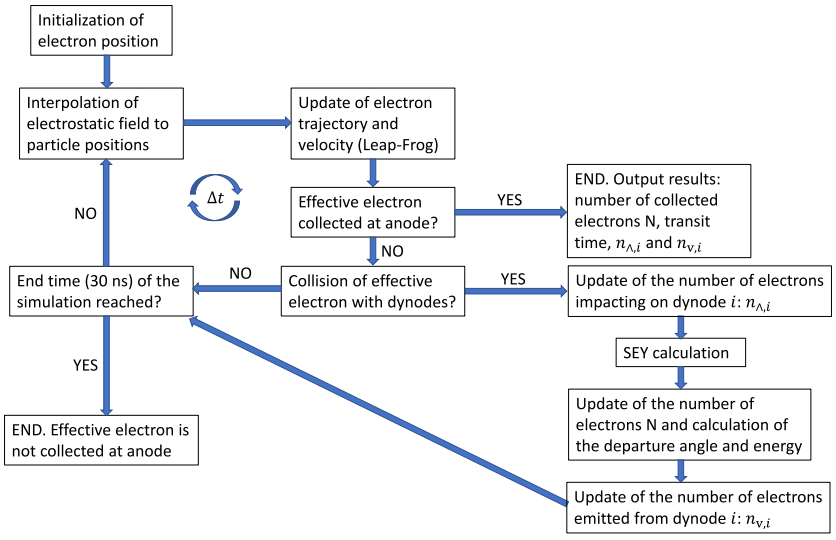

Fig. 3. Simulation code flowchart for each electron emitted from the photocathode. We deploy an in-house developed code written in MATLAB [16] by MathWorks (version 2022b). This includes the emission, transport with electrostatic field using Leap-Frog method assuming fixed voltages at electrodes and secondary electron emission if the particle impacts on an electrode.

The amplification is modeled considering one effective electron which represents a number N of real electrons that is updated after each impact. The parameter $\sigma_E = 2.2\,\text{eV}$ (fitted to the experimental results) is employed when the Rayleigh distribution is used to calculate the departure kinetic energy as $E_{out} = \sigma_E\sqrt{-2\ln u_1}$ [14], where $u_1 \in [0,1]$ is a random number. The direction of emission is obtained assuming a local spherical coordinate system centered at the impact point and calculating the polar angle θ_{out} (respect to the normal of the surface) and the azimuthal angle φ_{out} using the 3D cosine law $\theta_{out} = \arcsin(\sqrt{u_2})$ [22], and a uniform probability density $\varphi_{out} = 2\pi u_3$, respectively, where $u_i \in [0,1]$ are random numbers.

3.1.4. Collection

As the simulations are based on an effective model, we obtain the time that the lth original emitted electron takes to arrive to the anode and the number of electrons $n^l_{\wedge,N+1}$ that it represents. A total of $N_T = 20\,000$ electrons are emitted (uniformly distributed) from the photocathode; thus, the Gain is given by

$$\text{Gain} = \frac{\sum_{l=1}^{L} n^l_{\wedge,N+1}}{N_T}, \tag{6}$$

where $L \le N_T$ is the number of effective electrons that are collected in the anode. The temporal figures of merit of the PMT are obtained by fitting a Gaussian curve to the histogram of the number of collected electrons as a function of transit time.

3.2. Simulation of the resistive divider network

Because the PMT electrodes are not supplied individually with independent voltage sources, but indirectly with a single voltage supply and a passive divider network, there is no assurance that the voltages at the electrodes are stable unless the tube is in complete darkness.

The flow of electrons in the vacuum tube behaves as a current source, which acts simultaneously to the voltage supply source. Hence, the electrode currents going through each electrode towards the voltage divider can disturb the dynode voltages, as seen in Eq. (5), and, consequently, modify the gain of the PMT.

This effect is taken into account following an iterative simulation strategy. First, we perform a simulation neglecting this effect (i.e. using the nominal dynode voltages for the electrostatic field solution) and we calculate the mean number of electrons $\bar{n}_{\wedge,i}$ that impact on each electrode i and the mean number of electrons $\bar{n}_{v,i}$ that are emitted from each electrode i per electron emitted from the cathode. As we simulate N_T independent electrons emitted from the cathode:

$$\bar{n}_{\wedge,i} = \frac{\sum_{l=1}^{N_T} n^l_{\wedge,i}}{N_T}, \tag{7}$$

$$\bar{n}_{v,i} = \frac{\sum_{l=1}^{N_T} n^l_{v,i}}{N_T}, \tag{8}$$

where $n^l_{\wedge,i}$ ($n^l_{v,i}$) are the number of electrons impacting on (emitted from) dynode i for the lth emitted electron from the cathode, cf. Fig. 3. Therefore, the current flowing through each dynode, cf. Eq. (3), is given by $I_{dy,i} = e(\bar{n}_{v,i} - \bar{n}_{\wedge,i})\phi_k = -(\bar{n}_{v,i} - \bar{n}_{\wedge,i})I_k$.

Once the electrode currents are obtained, Eq. (5) is a linear system that can be easily solved to obtain the dynode voltages, as compared to [7] where the currents are unknown and the system is non-linear. Then, the electrostatic fields are calculated and the simulation repeated for these new electrode voltages. New values for $\bar{n}_{v,i}$, $\bar{n}_{\wedge,i}$ and $I_{dy,i}$ are obtained, as well as for the dynode voltages when solving Eq. (5). This procedure is repeated iteratively until the voltages converge as depicted in a flowchart in Fig. 4(a). We use the following convergence criterion: that the voltage of all the dynodes resulting from Eq. (5) differs by less than $\epsilon_V = 1\,\text{V}$ with respect to the voltages used for calculating the electrostatic fields of the current iteration of the simulation.

The direct convergence is not ensured if I_k is high. For this reason, we consider the step value ΔI_k and we begin by solving $\tilde{I}_k = \Delta I_k$, then its solution is used as the initial dynode voltages to solve $\tilde{I}_k = 2\Delta I_k$ up to the desired value of $I_k = M\Delta I_k$ as depicted in a flowchart in Fig. 4(b). In some cases, it may be convenient to obtain the initial voltages from a linear extrapolation of those obtained in the two previous steps. Thus, we obtain a scan of the initial current emitted from the cathode in the range $[0, I_k]$ with steps ΔI_k. We typically use the step value $\Delta I_k = -1\,\text{pA}$, although for high supply voltages, smaller step

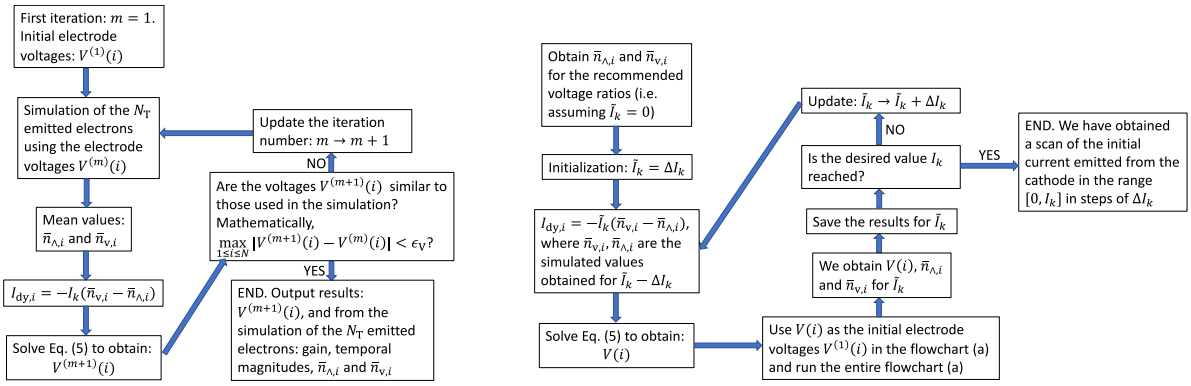

(a) Flowchart for a given I_k and supply voltage V_B (b) Flowchart for a scan in I_k for a given supply voltage V_B

Fig. 4. Simulation code flowcharts of the iterative method employed to take into account the resistive divider network. On the one hand, we have the iterative method to simulate a certain I_k providing initial values for the dynode voltages and, on the other hand, the iterative method to perform a scan in I_k starting from the nominal dynode voltages. The value $\epsilon_V = 1$ V is normally used in the convergence criterion.

values (in absolute value) are required. When the voltage of a dynode approaches zero, this iterative method may not converge and it is required during the simulations to maintain the voltage of that dynode within a small range of voltages and apply a kind of bisection method. Note that if a simulation is carried out and the currents obtained provide voltages sufficiently similar (i.e. that satisfy the convergence criterion) to those with which the simulation was performed, these voltages are the ones sought.

4. Experimental setup

Experimental measurements are taken using a Hamamatsu R13408-100 PMT with a magnetic shield, an isolated aluminum housing and an optic fiber feedthrough from Thorlabs (Newton, NJ, USA), assembled by Hilger Crystals (Margate, UK). The PMT was supplied with negative high voltage by an HVLAB3000 from ET Enterprises (Uxbridge, UK), with 1 V nominal precision and a maximum output power of 9 W. A PicoQuant Pulsed Diode Laser PDL 800-D operating at a repetition frequency of 125 kHz was used as a 650 nm photon source. The Direct current (DC)–coupled voltage divider Printed Circuit Board (PCB) was designed and manufactured by IGFAE with the resistor values shown in Table 1.

As a side note: it should be mentioned that the onset of gain drift effects at high photocathode currents is strongly dependent on the bleeder current, i.e. the current going through the resistors when no light impinges on the photodetector. With smaller resistor values, the effect would appear at larger photocathode currents (at the price of more temperature due to the Joule effect and potential additional noise due to the thermoelectrons [23]). The choice of 10 MΩ was for analogy with its active counterpart: the current development by IGFAE of a fully transistorized divider inspired by the ET enterprises design [24].

To monitor the dynode voltage in real-time, an additional PCB developed at IFIC was stacked on top of the divider. First, the voltage in each dynode was divided by a factor 500 using a through-hole resistor bridge of 5 GΩ (with high voltage rating) and two parallel 20 MΩ, cf. Fig. 5. The rationale of choosing the 5 GΩ resistor is to minimize the bias introduced by the monitoring in the voltage divider network (Table 1), whose effective resistance yields 149.6 MΩ. Second, the resulting voltage after the bridge (e.g. −3 V for −1500 V) is then inverted using a high-impedance operational amplifier LMC660 from Texas Instruments (Dallas, TX, USA) deployed with unity gain configuration.

The resulting output between 0 and 3 V (PMT supply between 0 and −1500 V) was digitized with an Arduino Due board from Arduino (Ivrea, Italy). This board hosts a SAM3X8EA microcontroller from Atmel (San Jose, CA, USA), featuring 12 channels on a 12-bit 1 Msps Analog to Digital Converter (ADC). Data were transferred to a computer through serial communication. The monitored voltage per channel was obtained as the median of all the collected values in an interval of about 2 s. A calibration of the raw ADC value and the PMT electrode voltage was performed separately for each channel. Furthermore, the small systematic bias introduced in the original voltage by the addition of 5 GΩ resistors in parallel with the 149.6 MΩ divider chain was simulated using Simulation Program with Integrated Circuit Emphasis (SPICE) and used as correction factor of the experimental measurements.

In addition, the anode signal was digitized with an 8-bit 2.5 GHz WaveRunner 625Zi oscilloscope from Teledyne Lecroy (Chestnut Ridge, NY, USA), operated at a sampling rate of 20 Gsps and with DC coupling (50 Ω), in parallel to the safety resistor of 10 MΩ to ground of the passive divider. Since the future intended application of this PMT (coupled to a scintillator) is for prompt gamma-ray detection in proton therapy with an acquisition system with 50 Ω impedance and zero dead time [25], we chose an equal DC-coupling impedance in the oscilloscope. Each data acquisition consisted of an average of 1 000 waveforms to minimize the statistical error and were processed off-line. The trigger was synchronized with the repetition frequency of the laser.

The obtained experimental data were used to validate the MC simulations as well as to compare with the theoretical expressions given in Section 2 assuming that the electrons emitted from the electrode i can only travel to the next dynode $i+1$ with an efficiency $\eta_i \equiv \xi_{i(i+1)}$ or be self-absorbed in the emitting dynode (i.e. $S_{ii} = 0$) with probability $\xi_{ii} \equiv 1 - \eta_i$. Therefore, the currents going through each dynode $I_{dy,i}$ appearing in Eq. (5) can be calculated from Eq. (3) as:

$$I_{dy,1} = -I_k\eta_0(S_{01}\eta_1 - 1), \quad I_{dy,i} = -I_k\eta_0\left(\prod_{j=1}^{i} S_{j(j+1)}\eta_j - \prod_{j=1}^{i-1} S_{j(j+1)}\eta_j\right), \quad i \in [2, N]. \tag{9}$$

In particular, we assume efficiencies $\eta_i = 1$ for all but the last two dynodes (7 and 8), which can be described by a logistic function:

$$\eta_i = \frac{1}{1 + \exp[B_i - (V(i+1) - V(i))]} \quad i \in [7, 8], \tag{10}$$

as was proposed in [7] to avoid non-physical voltages at the last dynodes. We chose $B_7 = 45$ V and $B_8 = 1$ V in Eq. (10) to empirically fit the experimental measurements.

We calculated the SEY as[2] $S_{ji} = kV_{ji}^{\alpha}$ where $V_{ji} = V(i) - V(j)$ and $k = 0.141487$, $\alpha = 0.721875$ for numerically solving the system of non-linear equations, Eqs. (5), as was described in [7]. Although this expression

[2] In our previous publication [14] the notation was instead rE^{β}. Here, we abbreviate it as k^{α} model.

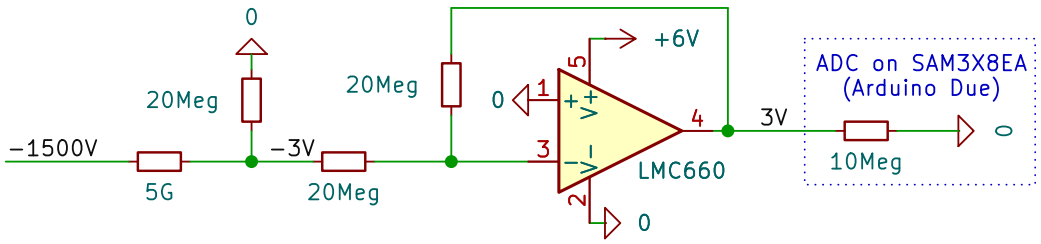

Fig. 5. Schematic of one of the twelve channels of the high-impedance circuit designed to monitor the high voltage of an electrode of the PMT without disturbing the original voltages supplied by the passived divider network. The electrode voltage at −1500 V is divided by 500 and inverted to match the +3 V maximum input range of the digitizer on the Arduino Due.

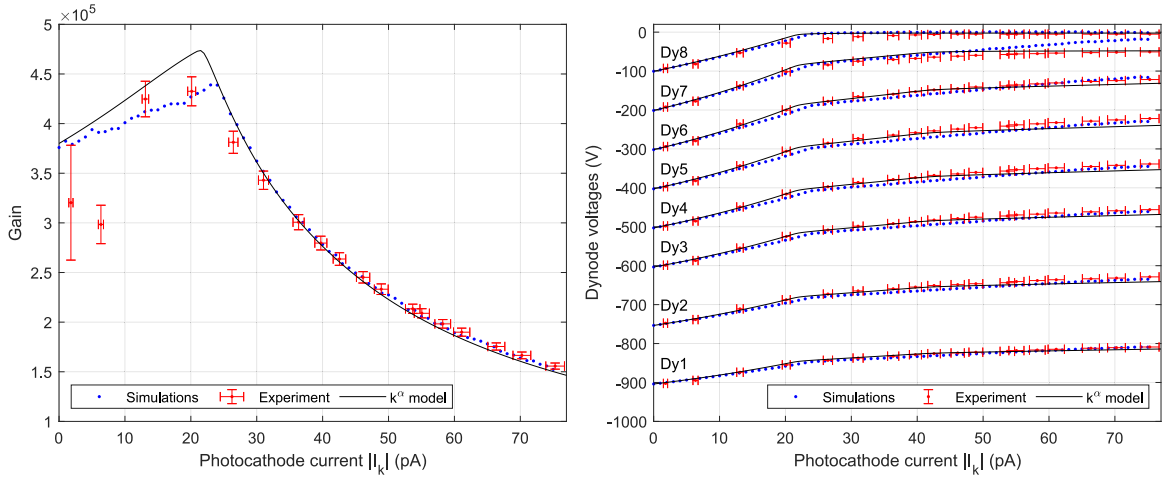

(a) Gain (b) Dynode voltages

Fig. 6. Comparison of the gain and dynode voltages obtained in the simulations, experimental measurements and the analytical model as a function of the photocathode current for a voltage bias $V_B = 1500$ V.

is a simplification that does not reproduce the shape of the actual SEY curves [14, Fig. 3] and does not take into account the impacting incidence angle, it is typically able to provide results which agree with the simulations and experimental measurements. In section SA of the Supplementary material, we have considered the Modified Vaughan's model for the SEY calculation (as in the simulations) for numerically solving the system of non-linear equations, obtaining similar results as with the k^α model.

5. Results and discussion

5.1. Gain and dynode voltages

Fig. 6 shows the gain and the dynode voltages as a function of the photocathode current for a voltage bias $V_B = 1500$ V (qualitatively similar results but worse quantitative agreements are obtained at a voltage bias of 1000 V, see section SD of Supplementary material). It can be seen that the gains obtained with the simulations, experiment and analytical model are in good agreement (the average percentage deviation of the experimental measurements with respect to the simulations and the analytical model is ∼3.7%), except for low photocathode currents where the measured signal to noise ratio is rather small because of the small pulse amplitudes. For low photocathode currents ($|I_k| \lesssim 20$ pA), the inter-dynode voltages increase slightly with the photocathode current except the inter-dynode voltage between dynode 7 and dynode 8 which decreases slightly (similarly to Figure 6(b) in [7]), whose combined effect produces an increase of the gain. If $|I_k| > 22$ pA, the gain quickly diminishes because the voltage at dynode 8 approaches zero, resulting in a significant drop in the efficiency of electrons going from the last dynode to the anode (cf. section SB of Supplementary material) which becomes the dominating factor in Eq. (4). This behavior of the gain is predicted by the analytical model (i.e. solving the Kirchhoff's equations and considering a gain that depends on the inter-dynode voltage) if the logistic function is considered. In fact, a qualitatively similar behavior was observed in [7]. On the other hand, the dynode voltages are satisfactorily described with the three methods (the average absolute deviation of the experimental measurements with respect to the simulations and the analytical model is ∼8 V and ∼5 V, respectively), although the simulations predict that the dynode 7 should get closer to the voltage of dynode 8 for high currents.

Fig. 7 depicts the gain and the dynode voltages as a function of the voltage bias for different photocathode currents. It can be seen that typically the gain decreases if the photocathode current increases. Furthermore, there is a saturation for high voltages which becomes more important and appears for smaller voltages for higher photocathode currents. In general, there is a moderate agreement between the simulations, experimental measurements and the analytical model (the average percentage deviation of the experimental measurements with respect to the simulations and the analytical model are ∼24% and ∼35%, respectively, for the three photocathode currents). It is worth mentioning that the higher gain experimentally obtained for low voltages is probably due to an underestimation of the SEY curve of the materials for small impacting energies, as was mentioned in [14]. The experimental dynode voltages are adequately explained by the simulations and the analytical model, although there are small discrepancies

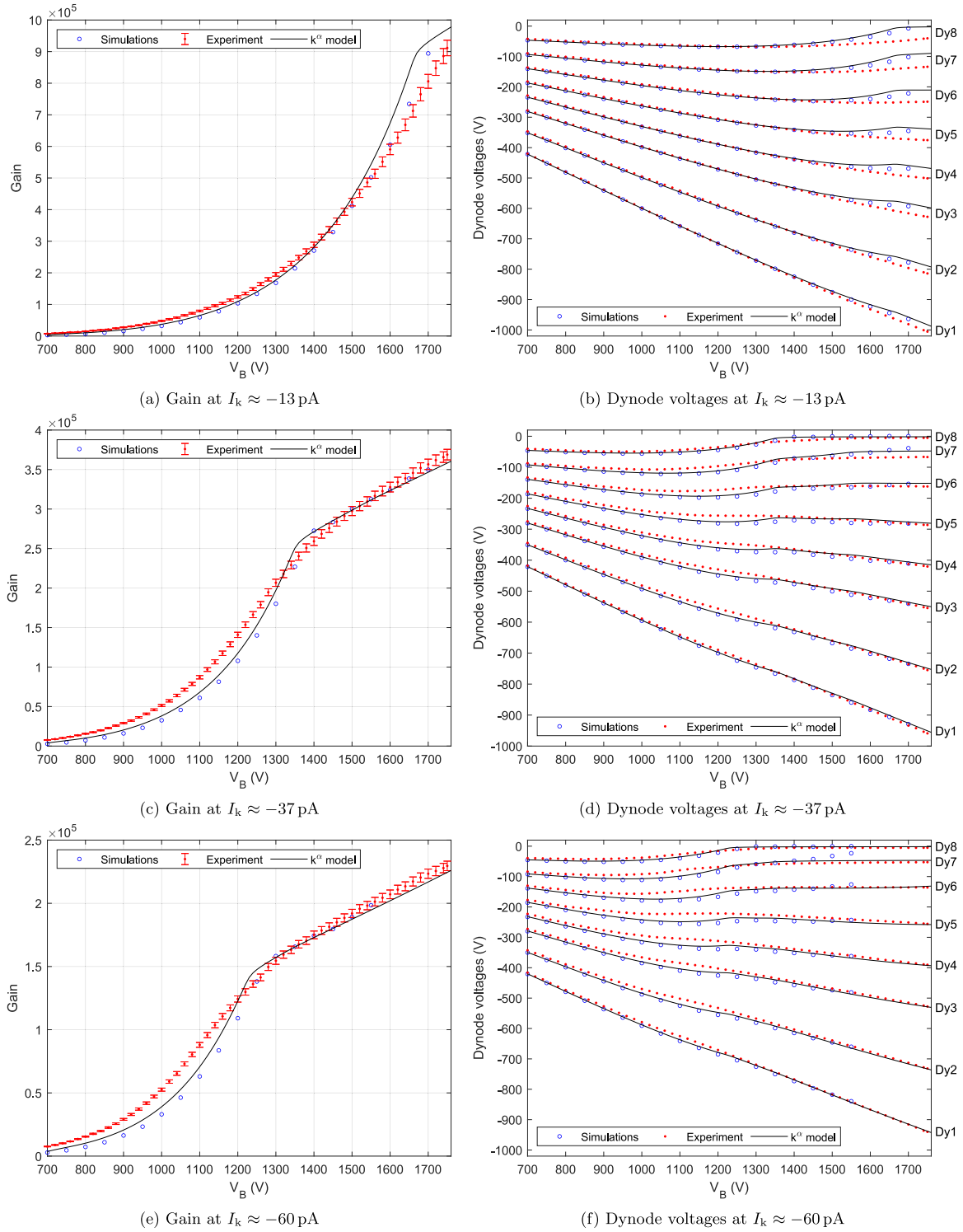

(a) Gain at $I_k \approx -13\,\text{pA}$ (b) Dynode voltages at $I_k \approx -13\,\text{pA}$

(c) Gain at $I_k \approx -37\,\text{pA}$ (d) Dynode voltages at $I_k \approx -37\,\text{pA}$

(e) Gain at $I_k \approx -60\,\text{pA}$ (f) Dynode voltages at $I_k \approx -60\,\text{pA}$

Fig. 7. Comparison of the gain and dynode voltages obtained in the simulations, experimental measurements and the analytical model as a function of the voltage bias for different photocathode currents: −13 pA, −37 pA and −60 pA. For $I_k \approx -60\,\text{pA}$ the simulations do not converge properly for high voltages and, for this reason, are not plotted for $V_B \geq 1600\,\text{V}$.

for high voltages for $I_k \approx -13\,\text{pA}$ and in the range $V_B \in [900, 1300]\,\text{V}$ for the other values of I_k, where the experimental values are higher than the ones obtained with the other methods. Numerically, the mean absolute error of all dynode voltages between the experiment and the simulations and the analytical model is $\sim 9\,\text{V}$.

5.2. Rise and transit time

We have studied the dependence of the PMT temporal magnitudes on the photocathode current. Fig. 8 illustrates the relationship between the photocathode current and both the simulated and experimental rise

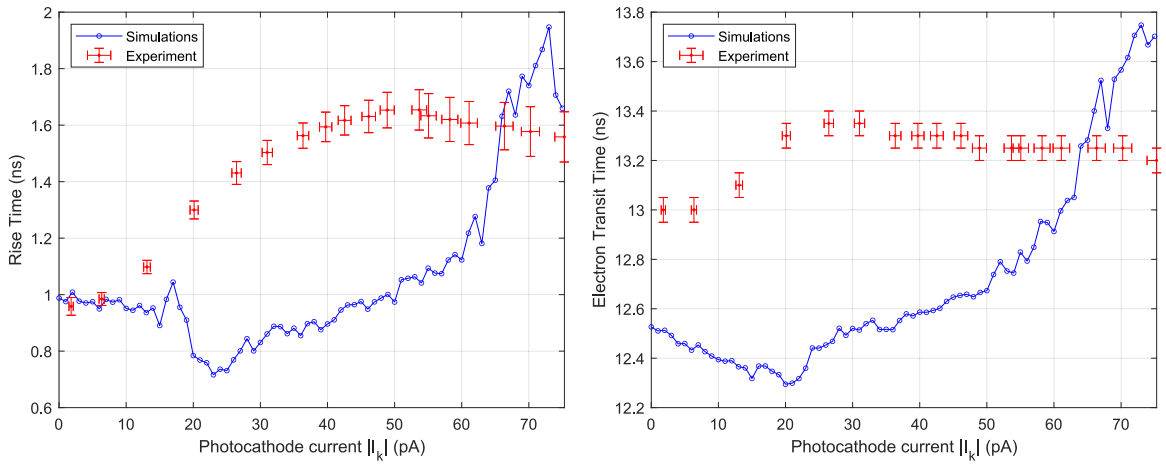

(a) Rise time (b) Electron transit time

Fig. 8. PMT temporal magnitudes obtained in the simulations and the experimental measurements as a function of the photocathode current for a voltage bias $V_B = 1500$ V.

time and electron transit time. Regarding the rise time, it can be seen that they have similar values for very small photocathode currents, but the simulated values, in general, decrease up to $|I_k| \approx 23$ pA, whereas the experimental values increase monotonically. Then, in the intermediate region $|I_k| \in [23, 50]$ pA, both experimental and simulated values increase, but simulations predict a value ≈ 0.6 ns smaller. For the higher photocathode currents, the experimental rise time remains approximately constant contrary to the simulations, which predict a rapid increase (i.e. a degradation of the pulse). This degradation may be explained because many electrons experience several bounces on dynode 8 since the difference of voltage between dynode 8 and anode is very small (cf. section SB of Supplementary material). The simulated and experimental values of the electron transit time have a similar behavior compared to the rise time. In general, the mean error between simulations and experiment is ~ 0.45 ns in the rise time and ~ 0.58 ns in the transit time. It is worth mentioning that the numerical values do not agree for $|I_k| \to 0$ because the simulations are performed with the 2.5D strategy which underestimates this magnitude.

Fig. 9 compares the simulated and experimental rise time and electron transit time for different photocathode currents as a function of the voltage bias. We can see a good agreement in the rise time for the lowest photocathode current: $|I_k| \approx 13$ pA (mean error of ~ 0.12 ns in the rise time and ~ 0.48 ns in the transit time). For higher $|I_k|$, the simulations predict an increase of the rise time for high voltages, while the measurements show that this increment occurs for smaller voltages and even the rise time begins to decrease for higher voltages. Regarding the electron transit time, in addition to the displacement due to the use of the 2.5D strategy, we can see that both simulations and experimental measurements show an increase of the transit time when the photocathode current increases. Similarly to the rise time, this behavior begins for smaller voltages in the experimental measurements compared to the simulations. Numerically, for $|I_k| \approx 37$ pA and $|I_k| \approx 60$ pA the mean error in the rise time is ~ 0.41 ns and ~ 0.68 ns in the transit time.

Thus, we have seen that the simulations are not able to predict the experimental temporal magnitudes with high accuracy if the photocathode current and/or the voltage bias are sufficiently high. In those cases, the number of electrons that make up the avalanche within the PMT becomes huge, with peak anode current of over 10 mA. Here, we expect that the high voltage supply maximum current limitation circuit affects the measurement, with some transient effects due to the internal capacitors, that are not modeled analytically nor in the simulations. In fact, at high peak anode currents (above 12 mA, especially for measurements at > 1200 V) we observe periodic oscillations in the electrode voltages measured with the Arduino Due board, with a frequency of $\sim$4 Hz and amplitude of $\sim$5 V around the mean value. Note that this oscillation frequency is completely unrelated to the pulse repetition frequency of 125 kHz.

Additionally, space-charge effects may modify the electron motion, degrading the pulse shape. This effect is not included in the simulations and may contribute to the discrepancies between the simulations and experimental measurements.

5.3. Novelty and limitations

Compared to previous literature on PMT equivalent circuit models [7,26], experimental validation [10] and MC simulations [13,14], our study incorporates the following innovations:

1. our generalized analytical model considers a correlation matrix ξ_{ji} to take into account that electrons can travel between any electrode pairs, not only from one electrode to the subsequent one in the ladder (a diagonal matrix). We then later verify that, for our PMT and setup, the diagonal approximation is valid except for the last two dynodes.
2. our framework couples the MC simulations with the actual resistances in the divider circuit, thus providing more realistic results. It calculates the electrostatic field solution and reruns the simulation based on the electrode voltages resulting from solving the system of Eqs. (5), whose variables depend on the resistors and on the previous iteration of the simulation (the currents flowing through to the electrodes during the transport and amplification of the electrons within the device);
3. our simulations have demonstrated that the analytical model may use the k^α approximation without loss of precision, but that it needs to incorporate a logistic function to characterize the efficiencies η_i of the last two dynodes in order to have a good agreement with the experimental measurements, as was predicted in [7];
4. numerous validation experiments have been carried out for several voltages, intensities and with high-resolution steps, monitoring in real-time each electrode voltage, the gain, electron rise time and electron transit time. In particular, we have demonstrated that the gain and the dynode voltages (in absolute value) decrease for high photocathode currents, in analogy to the saturation of the gain at higher voltages that was experimentally found in [14].

Among the limitations, both the analytical model and the Monte Carlo simulation do not include transient effects but only steady-state solutions; likewise, our experimental voltage divider has no capacitors

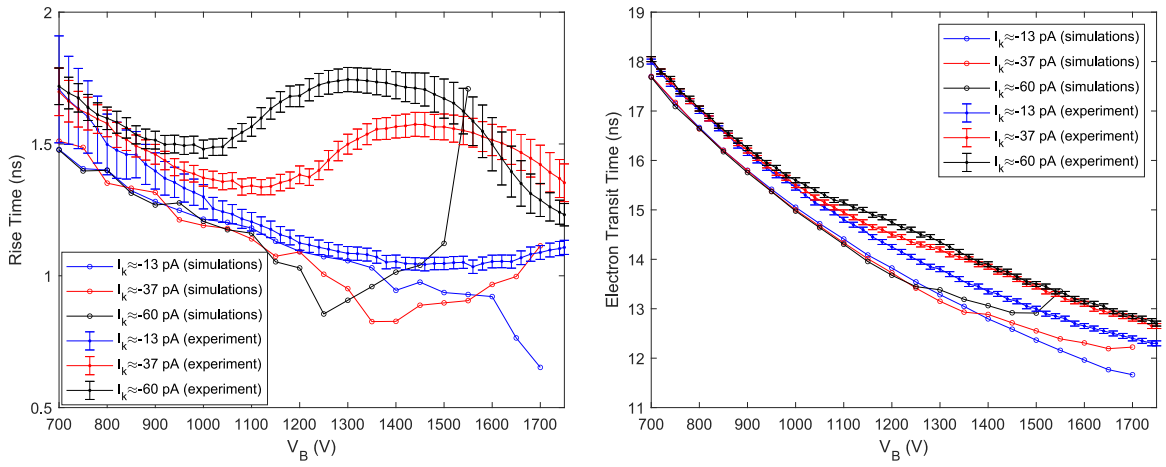

(a) Rise time (b) Electron transit time

Fig. 9. PMT temporal magnitudes obtained in the simulations and the experimental measurements as a function of the voltage bias for different photocathode currents.

inserted in any electrode stage (other than builtin capacitors of the external voltage supply). Actually, capacitors and transistors are usually added to the voltage dividers to mitigate the gain drift effects. This would however have a dramatic impact on the computational load of the model and MC simulations. Furthermore, the maximum current limitation circuit of the HVLAB3000 voltage supply has not been modeled.

Although a continuous wave laser could have been used for a more adequate comparison between the experimental measurements and the simulations (where a mean steady-state photocathode current is assumed), we have chosen a pulsed laser, since it resembles better the illumination conditions when coupling fast scintillation crystals with a PMT, as well as the resulting gain drifts published in the literature [3].

It is also worth mentioning that an inaccurate 3D geometry of the PMT may add systematic errors in the MC simulation. Finally, space-charge effects are not accounted for, even if they may have an impact at very high voltages and photocathode intensities, especially in the region between dynode 7, dynode 8 and the anode. We have started investigations in this direction [27], as the formula of Ackerstaff et al. [28] predicts that space charge may start to be important at 6 mA anode current for this geometry (assuming that dynode 8 and anode are plane-parallel electrodes with area 60 mm^2, distance 0.5 mm and a voltage difference of 5 V).

6. Conclusions

In this work, we have proposed a general analytical model to describe the effect of the currents flowing through the passive divider network as a result of illuminating the PMT. Furthermore, we have described an iterative procedure that couples Monte Carlo numerical simulations with the voltage drifts predicted according to the resistors used in the divider.

The simulations have been compared with experimental measurements and the analytical model obtaining a good quantitative agreement in terms of gain and dynode voltages, and a moderate one in terms of electron rise time and transit time. It has been shown that even a simple SEY model, such as the k^{α} model, is capable of providing accurate results, but that logistic functions need to be introduced to take into account the collection efficiency in the last dynodes.

Future work will be devoted to modeling transient effects and active voltage dividers, and to the research of space-charge effects, which may become relevant at high photocathode currents and/or supply voltages, especially for pulsed regimes such as prompt gamma-ray imaging in proton therapy.

CRediT authorship contribution statement

Pablo Martín-Luna: Writing – review & editing, Writing – original draft, Validation, Software, Methodology, Investigation, Formal analysis, Data curation, Conceptualization. **Daniel Esperante:** Writing – review & editing, Supervision, Methodology, Conceptualization. **José Vicente Casaña:** Writing – review & editing, Resources, Methodology. **Antonio Fernández Prieto:** Writing – review & editing, Resources. **Nuria Fuster-Martínez:** Writing – review & editing, Supervision, Funding acquisition. **Iris García Rivas:** Writing – review & editing, Resources. **Benito Gimeno:** Writing – review & editing, Supervision, Methodology, Conceptualization. **Damián Ginestar:** Writing – review & editing, Software, Methodology. **Daniel González-Iglesias:** Writing – review & editing, Supervision, Software, Conceptualization. **José Luis Hueso:** Writing – review & editing, Software, Methodology. **Hannah Andrea Leptin:** Writing – review & editing, Data curation. **Gabriela Llosá:** Writing – review & editing, Supervision, Funding acquisition. **Pablo Martinez-Reviriego:** Writing – review & editing, Supervision. **Jaime Riera:** Writing – review & editing, Software, Methodology. **Pablo Vázquez Regueiro:** Writing – review & editing, Supervision, Resources. **Fernando Hueso-González:** Writing – review & editing, Writing – original draft, Validation, Software, Project administration, Methodology, Investigation, Funding acquisition, Data curation, Conceptualization.

Declaration of competing interest

The authors declare that they have no known competing financial interests or personal relationships that could have appeared to influence the work reported in this paper.

Acknowledgments

This work was supported by Conselleria de Educación, Investigación, Cultura y Deporte (Generalitat Valenciana), Spain under grant numbers CDEIGENT/2019/011 and CDEIGENT/2021/012. This work has also received financial support through funds from the Industrial Doctorates program from the Xunta de Galicia (Galician Innovation Agency), Spain. P. Martín-Luna is supported by the Ministerio de Universidades (Gobierno de España), Spain under Grant Number FPU20/04958. We thank Hamamatsu (V. Sánchez, D. Castrillo) for technical support and guidance; R. Carrasco (IFIC) and P. Wohlfahrt (Siemens Healthineers) for the CT scanning; the electronics, mechanics,

informatics, maintenance services at IFIC, as well as the Scientifc Unit for Business Innovation (UCIE) for excellent support; and K. Albiol, D. Calvo, J. Collado Ruiz, A. Delgado Belmar, A. Gallas Torreira, C. García, E. Lemos Cid, E. Nácher, G. Pausch, A. Pazos Álvarez, E. Pérez Trigo, D. Real, S. Rit, A. Ros, J. Roser, C. Senra, J. Stein, J. L. Taín and R. Viegas for useful discussions.

Appendix A. Supplementary data

Supplementary material related to this article can be found online at https://doi.org/10.1016/j.sna.2024.116057.

Data availability

Data will be made available on request.

References

[1] A.G. Wright, The Photomultiplier Handbook, Oxford University Press, 2017, http://dx.doi.org/10.1093/oso/9780199565092.001.0001.

[2] Hamamatsu Photonics K. K., Photomultiplier tubes. Basics and applications, fourth ed., 2017, URL https://www.hamamatsu.com/resources/pdf/etd/PMT_handbook_v4E.pdf.

[3] T. Werner, J. Berthold, F. Hueso-González, J. Petzoldt, K. Roemer, C. Richter, A. Rinscheid, A. Straessner, W. Enghardt, G. Pausch, Processing of prompt gamma-ray timing data for proton range measurements at a clinical beam delivery, Phys. Med. Biol. 1 (10) (2019) 105023, http://dx.doi.org/10.1088/1361-6560/ab176d.

[4] F. Hueso-González, M. Rabe, T.A. Ruggieri, T. Bortfeld, J.M. Verburg, A full-scale clinical prototype for proton range verification using prompt gamma-ray spectroscopy, Phys. Med. Biol. 63 (18) (2018) 185019, http://dx.doi.org/10.1088/1361-6560/aad513.

[5] S.O. Flyckt, C. Marmonier, Photomultiplier tubes: principles and applications; 2nd ed., Photonis, Brive-la-Gaillarde, France, 2002, URL https://www2.pv.infn.it/~debari/doc/Flyckt_Marmonier.pdf.

[6] G. Lachs, The statistics for the detection of light by nonideal photomultipliers, IEEE J. Quantum Electron. 10 (8) (1974) 590–596, http://dx.doi.org/10.1109/JQE.1974.1068206.

[7] F. Hueso-González, D. Ginestar, J.L. Hueso, J. Riera, Comments on "SPICE model of photomultiplier tube under different bias conditions", IEEE Sens. J. 21 (15) (2021) 17395–17402, http://dx.doi.org/10.1109/JSEN.2021.3062428.

[8] D. Yu Akimov, E.S. Kozlova, Y.A. Melikyan, Computer modelling of the Hamamatsu R11410-20 PMT, J. Phys. Conf. Ser. 798 (2017) 012211, http://dx.doi.org/10.1088/1742-6596/778/1/012211.

[9] J. Peña-Rodríguez, S. Hernández-Barajas, Y. León-Carreño, L.A. Núñez, Modeling and simulation of the R5912 photomultiplier for the LAGO project, IEEE Sens. J. 21 (18) (2021) 20184–20191, http://dx.doi.org/10.1109/JSEN.2021.3096426.

[10] M. Heifets, P. Margulis, Fully active voltage divider for PMT photo-detector, in: IEEE Nucl Sci Symp Conf Rec, 2012, pp. 807–814, http://dx.doi.org/10.1109/NSSMIC.2012.6551216.

[11] G. Pausch, J. Berthold, W. Enghardt, K. Roemer, A. Straessner, A. Wagner, T. Werner, T. Koegler, Detection systems for range monitoring in proton therapy: Needs and challenges, Nucl. Instr. Methods Phys. Res. A 954 (2018) 161227, http://dx.doi.org/10.1016/j.nima.2018.09.062.

[12] F. Hueso-González, T. Bortfeld, Compact method for proton range verification based on coaxial prompt Gamma-ray monitoring: a theoretical study, IEEE TRPMS 4 (2) (2020) 170–183, http://dx.doi.org/10.1109/TRPMS.2019.2930362.

[13] J. Beavers, K. Huddleston, N. Hines, W. McNeil, Modeling electron transport and multiplication in photomultiplier tubes using COMSOL Multiphysics®, J. Instrum. 17 (12) (2022) P12015, http://dx.doi.org/10.1088/1748-0221/17/12/P12015.

[14] P. Martín-Luna, D. Esperante, A. Fernández Prieto, N. Fuster-Martínez, I. García Rivas, B. Gimeno, D. Ginestar, D. González-Iglesias, J.L. Hueso, G. Llosá, P. Martinez-Reviriego, A. Meneses-Felipe, J. Riera, P. Vázquez Regueiro, F. Hueso-González, Simulation of electron transport and secondary emission in a photomultiplier tube and experimental validation, Sensors Actuators A 365 (2024) 114859, http://dx.doi.org/10.1016/j.sna.2023.114859.

[15] FreeCAD 0.20, 2022, URL https://www.freecad.org/index.php.

[16] MATLAB (R2022b), 2022, URL https://es.mathworks.com/products/matlab.html.

[17] K. Halbach, R.F. Holsinger, Superfish -a computer program for evaluation of RF cavities with cylindrical symmetry, Part. Accel. 7 (1976) 213–222, URL https://inspirehep.net/files/76ad49d27c8d9b6069ed25b6c67b44b0.

[18] B. Ripperda, F. Bacchini, J. Teunissen, C. Xia, O. Porth, L. Sironi, G. Lapenta, R. Keppens, A comprehensive comparison of relativistic particle integrators, Astrophys. J. Suppl. Ser. 235 (1) (2018) 21, http://dx.doi.org/10.3847/1538-4365/aab114.

[19] J.P. Boris, Relativistic plasma simulation-optimization of a hybrid code, in: Proc. Fourth Conf. Numerical Simulations of Plasmas (Washington, D.C.: Naval Research Laboratory), 1970, pp. 3–67, URL https://apps.dtic.mil/sti/citations/ADA023511.

[20] J. Vaughan, A new formula for secondary emission yield, IEEE Trans. Electron Devices 36 (9) (1989) 1963–1967, http://dx.doi.org/10.1109/16.34278.

[21] C. Vicente, M. Mattes, D. Wolk, B. Mottet, H. Hartnagel, J. Mosig, D. Raboso, Multipactor breakdown prediction in rectangular waveguide based components, in: IEEE MTT-S International Microwave Symposium Digest, 2005., 2005, pp. 1055–1058, http://dx.doi.org/10.1109/MWSYM.2005.1516852.

[22] J. Greenwood, The correct and incorrect generation of a cosine distribution of scattered particles for Monte-Carlo modelling of vacuum systems, Vacuum 67 (2) (2002) 217–222, http://dx.doi.org/10.1016/S0042-207X(02)00173-2.

[23] B. Moritz Veit, Active voltage dividers for photomultipliers, 2019, 6th EABI-WG meeting, URL https://indico.cern.ch/event/800973/contributions/3328661/attachments/1804539/2944423/bveit_eabi_wb_active_voltage_dividers.pdf.

[24] P.G. Banks, A. Nikitin, J.D. Pizzey, A.G. Wright, multi-channel high voltage and control system for photomultipliers, Tech. rep, ET Enterprises Ltd, 2011, 2011, URL https://et-enterprises.com/images/technical_papers/rp097_multi-channel_high_voltage_and_control_system_for_PMTs.pdf.

[25] F. Hueso-González, J.V. Casaña Copado, A. Fernández Prieto, A. Gallas Torreira, E. Lemos Cid, A. Ros García, P. Vázquez Regueiro, G. Llosá, A dead-time-free data acquisition system for prompt gamma-ray measurements during proton therapy treatments, Nucl. Instrum. Methods Phys. Res. A 1033 (2022) 166701, http://dx.doi.org/10.1016/j.nima.2022.166701.

[26] N. Krihely, SPICE model of photomultiplier tube under different bias conditions, IEEE Sens. J. 14 (10) (2014) 3606–3610, http://dx.doi.org/10.1109/JSEN.2014.2329181.

[27] D. Esperante, B. Gimeno, D. Ginestar, J.H. D. González-Iglesias, F. Hueso-González, G. Llosá, P. Martín-Luna, J. Riera, Effect of electron space-charge on the gain of a two-dimensional photomultiplier tube model, in: Proceedings of Mathematical Modelling in Engineering & Human Behaviour, MME&HB2023, 2023, pp. 10–19, URL https://imm.webs.upv.es/jornadas/2023/home.html.

[28] K. Ackerstaff, J. Bisplinghoff, R. Bollmann, P. Cloth, F. Dohrmann, O. Diehl, G. Dorner, V. Drüke, H. Engelhardt, S. Eisenhardt, J. Ernst, P. Eversheim, D. Filges, S. Fritz, M. Gasthuber, R. Gebel, A. Gross, R. Gross-Hardt, F. Hinterberger, R. Jahn, U. Lahr, R. Langkau, G. Lippert, T. Mayer-Kuckuk, R. Maschuw, G. Mertler, B. Metsch, F. Mosel, H. Paetz gen. Schieck, H. Petry, D. Prasuhn, B. v. Przewoski, M. Radtke, H. Rohdjess, D. Rosendaal, P. von Rossen, H. Scheid, N. Schirm, F. Schwandt, W. Scobel, D. Theis, J. Weber, W. Wiedmann, K. Woller, R. Ziegler, Reduction of space charge effects and tests of larger samples of photomultipliers for the EDDA experiment, Nucl. Instr. Methods Phys. Res. A 335 (1) (1993) 113–120, http://dx.doi.org/10.1016/0168-9002(93)90262-G.

Pablo Martín-Luna received the degree in physics and the master's degree in advanced physics from the University of Valencia, Valencia, Spain, in 2020 and 2021, respectively, where he is currently pursuing the Ph.D. in physics. His current research interests include numerical simulations of the relativistic dynamics of charged particles in electromagnetic fields and the study of novel particle acceleration techniques using carbon nanostructures.

Daniel Esperante is an applied scientist (Telecommunications Engineering and Ph.D. in Physics) with a large international experience in R&D in instrumentation for particle physics experiments and Radio-Frequency (RF) accelerators. He has played a leading role in the coordination, design, development and commissioning of scientific instrumentation and complex electronic systems at various particle physics experiments and accelerators facilities. Currently he is the scientific responsible of design and commissioning of the IFIC's high-gradient Radio-Frequency laboratory for medical accelerators and other applications.

José Vicente Casaña received his Degree in Telecommunications Electronic Engineering and a Master's Degree in Telecommunications Engineering from the University of Valencia, Spain, in 2017 and 2019, respectively. Since 2019, he has been working as an electronic engineer at the IRIS group (Image Reconstruction, Instrumentation and Simulations for medical imaging applications), focused on the development and testing of electronics for SiPMs and silicon detectors to track the direction and energy of various physics particles.

Antonio Fernández Prieto holds a B.S. degree in Industrial Electronics from the University of León and a Ph.D. in Information Technology Research from the University of Santiago de Compostela. He is currently a researcher affiliated with the Galician Institute for High Energy Physics (IGFAE) and the European Organization for Nuclear Research (CERN). His main research interests include data acquisition systems, electronics design for photodetectors and silicon pixel detectors, as well as the integration of components within complex system architectures.

Nuria Fuster-Martínez received the Licenciado degree in physics, the master's degree in advanced physics and the Ph.D. in physics from the University of Valencia, Valencia,

Spain, in 2011, 2012 and 2017, respectively. She has a large international experience in beam dynamics simulations of charged particle beams in accelerators; calculation of impedances and wakefields in accelerator structures; beam operation in linear and circular high-energy accelerators; and beam instrumentation R&D for linear colliders. Since 2020 she is focusing her research activities on accelerator applications in medicine, in particular, in high-gradient accelerators physics and technology and novel radio-therapy techniques.

Iris García Rivas is a PhD student in Nuclear and Particle Physics. After finishing her studies in Physics with the specialization in Nuclear Physics, she started to work in the Galician Institute of High Energy Physics (and in collaboration with the Institute for Corpuscular Physics, Valencia) within the framework of the development of a novel detection system for proton therapy treatments monitoring. More recently, she started her Ph.D. program in the University of Santiago de Compostela in consortium with the company TripleAlpha Innovation to continue contributing to this promising project.

Benito Gimeno received the Licenciado degree in physics and the Ph.D. degree from the University of Valencia, Valencia, Spain, in 1987 and 1992, respectively. He became a Full Professor at the University of Valencia in 2010. His current research interests include the electromagnetic analysis and design of microwave passive components, RF breakdown high-power effects, particle accelerators for hadrontherapy, and dark matter axions search in the microwave frequency range.

Damián Ginestar earned his degree in Physics (1986) from Universitat de València (Spain) and his Ph.D. (1995) from the Universitat Politècnica de València (Spain). He works for the Applied Mathematics Department at the Universitat Politècnica de València (Spain) as full professor of Applied Mathematics and he is a member of the Instituto Universitario de Matemática Multidisciplinar. His research interests are many devoted to develop scientific computation methods applied to engineering problems, mainly related with nuclear reactor physics. Also he has performed some studies related with water and nitrogen dynamics in soils and with digital video analysis.

Daniel González-Iglesias received the Licenciado degree in physics, the master's degree in advanced physics and the Ph.D. in physics from the University of Valencia, Valencia, Spain, in 2010, 2011 and 2017, respectively. His current research interests include theoretical analysis of high-power phenomena (RF breakdown, multipactor) in microwave passive components for space communications systems and for particle accelerators applications, and the design of RF electron photoinjector guns for x-ray free electron lasers (FEL).

José L. Hueso earned his M.Sc. (1976) and Ph.D. (1984) in Mathematics from the Universitat de València (Spain). He has worked from 1976 to 2016 at the Universitat Politècnica de València (Spain) as associate professor of Applied Mathematics and has been a member of the Instituto Universitario de Matemática Multidisciplinar. His research interests include locally convex spaces, parallel computation, systolic algorithms, optical flow, local and semilocal convergence and dynamics of iterative method for nonlinear equations and systems and its application to economical models, and video analysis and simulation of physical processes.

Hannah Andrea Leptin is a bachelors student of Technical Physics at Technical University of Ilmenau, Germany. As part of her studies she did an internship at IFIC in Valencia where she was experimentally working on prompt gamma-ray imaging.

Gabriela Llosá has a Ph.D. in physics since 2005. She is a researcher at the Instituto de Física Corpuscular (IFIC), Valencia and the coordinator of the IRIS group (Image Reconstruction, Instrumentation and Simulations for medical imaging applications). She started her career in particle physics experiments and she has acquired a large international experience in detector development for medical applications. Her current research is focused on the development of medical imaging detectors and she is among the leading experts in Compton cameras. She is currently involved mainly in hadron therapy treatment monitoring and assessment of treatments with radiopharmaceuticals.

Pablo Martinez-Reviriego received the degree in physics from the University of Sevilla in 2019 and the master's degree in advanced physics from the University of Valencia in 2020, where he is currently pursuing the Ph.D. in physics. His current research interests include the studies of the viability of High-Gradient accelerator structures for their use in medical accelerators for hadrontherapy treatments in hospitals. In particular, he studies the non-linear phenomena such as RF breakdowns and dark currents, and their consequences in the accelerator cavities and their surroundings. Furthermore, he works on the RF design of Dielectric Loaded Accelerating structures for low beta particles.

Jaime Riera received his Ph.D. degree in Physics in 1990 from Universitat de València. He is a full professor in the Department of Applied Physics at the Universitat Politècnica de València (Spain). Dr. Riera has directed projects focused on the transmission of scientific knowledge through Information and Communication Technologies (ICTs). He has produced several documentaries on scientific subjects. He is currently researching at the Multidisciplinary Mathematics Institute, in the area of applications of image processing and digital tracking to medicine.

Pablo Vázquez Regueiro is Professor at U. Santiago de Compostela since 2013 with large background in particle detectors for High Energy Physics as the Silicon Tracker and the vertex detector for the LHCb experiment at CERN. He has expertise in silicon pixels, module production, quality assurance, electronics, detector commissioning or 4D tracking. Furthermore, he has produced a photodetector system based on APDs for quantum information processing and currently he is developing a new system for in vivo proton range verification with application in proton therapy treatments based on a scintillating crystal with a photomultiplier with active voltage divider and fast ADC.

Fernando Hueso-González did his Ph.D. on medical physics at Technische Universität Dresden thanks to a Marie Curie Early Stage Researcher fellowship, investigating on Compton cameras for proton therapy range verification. He then spent three years as a Postdoctoral Fellow at Harvard Medical School and Massachusetts General Hospital, working on the clinical translation of a collimated prompt gamma-ray camera from the lab bench to the proton treatment room. Currently, he is a Distinguished Researcher at IFIC leading a novel project on uncollimated prompt gamma-ray detection in a coaxial orientation.